Coactivation in symmetric four-bar mechanisms antagonistically actuated by cables

Vimalesh Muralidharan, Christine Chevallereau, Philippe Wenger

Coactivation in symmetric four-bar mechanisms antagonistically actuated by cables*

Vimalesh Muralidharan†, Christine Chevallereau, Philippe Wenger
Nantes Universite, Ecole Centrale de Nantes, CNRS, LS2N, 44321 Nantes, France
Email: m.vimalesh94@gmail.com, Christine.Chevallereau@ls2n.fr, Philippe.Wenger@ls2n.fr

ABSTRACT

In biological systems, the joints are actuated antagonistically by muscles that can be moved coherently to achieve the desired displacement and coactivated with appropriate forces to vary joint stiffness. Inspired by this, there is an interest in developing bio-inspired robots suitable for low- and high-stiffness tasks. Mechanisms actuated by antagonist cables can be a reasonable approximation of biological joints. A study on the anti-parallelogram mechanism showed that the antagonistic forces (>0) positively influence its stiffness, similar to the biological joints. This work investigates more general symmetric four-bar mechanisms with crossed/non-crossed limbs and top and base bars of unequal lengths for this property. Firstly, the cables are attached between the two unconnected pivot pairs in the four-bar mechanism, and their limits of movement are presented. Inside these limits, we show that the cable forces have a positive (resp. negative) influence on the stiffness of the mechanism when its limbs are crossed (resp. non-crossed). These results are validated experimentally in all cases. Subsequently, we consider alternate cable attachments for the mechanisms with non-crossed limbs to achieve coactivation. Examples show that coactivation is possible in these mechanisms but comes at the cost of a diminished range of movement. Among all the four-bar mechanisms considered, the anti-parallelogram mechanism offers the largest orientation range of $(-\pi,\pi)$ for the top bar w.r.t. its base while providing coactivation and is thus the best choice.

Nomenclature

l	Length of the two limbs of a symmetric four-bar mechanism
b	Length of the top bar/coupler of a four-bar mechanism
b_0	x-coordinate of a fixed pivot of a four-bar mechanism
C_1, C_2	Antagonist cables actuating a four-bar mechanism
l_1, l_2	Lengths of the antagnonist cables C_1, C_2, respectively
$D_1(x_d, y_d)$	Attachment point of the cable C_1 on the base
α	Orientation of the top bar of the four-bar mechanism w.r.t. its base
ϕ, ψ	Orientation of the two limbs of the four-bar mechanism w.r.t. its base
$\alpha_{\max}$	Upper bound for α due to geometry of the joint and cable actuation
F_1, F_2	Forces applied by the antagnonist cables C_1, C_2, respectively
K	Stiffness of the four-bar mechanism
γ_1, γ_2	Coefficients of the actuation forces F_1, F_2, in the respective expressions of stiffness

1 Introduction

There has always been an interest in developing robotic arms that are fast, accurate, repeatable, and energy-efficient for industrial applications. But, recently, research on robotic arms with more sophisticated capabilities, such as stiffness modulation, deployability, and safe interaction with the environment, has been gaining prominence [1], [2]. An important

*This article is an extended version of a paper presented at the 6th International Conference on Cable-Driven Parallel Robots (CableCon 2023) held at Nantes during 26-28 June 2023.

†Corresponding author

source of inspiration for developing such robots stems from the nature/biological systems, e.g., human arm in [3], giraffe's neck in [4], bird's neck in [5], elephant's trunk in [6].

One of the key differences between conventional robots and biological systems lies in their joints. While most of the robots are made up of revolute or prismatic joints, the biological systems hardly contain any of them. Instead, their joints are composed of complex surfaces in contact with one another. Some works have been dedicated exclusively to the study of kinematics of such joints, e.g., human knee in [7], [8]. The significance of closed kinematic chains in modeling biological movements is presented in [9]. A review of the animal joints and their approximation with linkage mechanisms can be found in [10].

Another interesting feature of biological joints is their actuation. Unlike conventional robots with linear or rotary actuators, they are actuated antagonistically by muscles. Typically, one set of muscle(s) contract while their antagonistic counterparts relax and vice versa to achieve the desired joint movement. However, under exceptional circumstances, both sets of muscles contract simultaneously to increase the stiffness of the joint. This phenomenon is referred to as the coactivation of muscles in biological systems [11]. This natural actuation scheme keeps the energy consumption at a minimum during regular operations and increases it through coactivation only while performing high-stiffness tasks. Inspired by this efficient scheme, variable stiffness actuators have been developed in [12], [13], where cables, along with non-linear springs, act as muscles to antagonistically actuate a pulley joint. The two cables are pulled (resp. released) simultaneously to increase (resp. decrease) the stiffness of this joint. However, it must be emphasized that this is possible for the pulley joint only in the presence of non-linear springs [12].

On the other hand, for tensegrity-inspired joints presented in [14], the stiffness modulation can be achieved by simply varying the cable forces without in-series springs. It was found that with the increase in antagonistic cable forces, the revolute joint experiences a drop in stiffness, which was a counter-intuitive result [14]. The same behavior was also reported for a 2R joint with offsets that represents one circle pure rolling over another [15]. In contrast, for an anti-parallelogram joint that is equivalent to one ellipse pure rolling over another, the antagonistic actuation has a positive influence on the joint stiffness [14], just as in the biological joints. Thus, drawing inspiration from the anti-parallelogram mechanism, this work aims to find all the four-bar mechanisms with symmetric limbs that exhibit coactivation.

We presented an initial version of this work in [16], showing that the four-bar mechanisms exhibit coactivation when their limbs are crossed but not otherwise. In this paper, we additionally provide experimental evidence for those results. Further, we also show that by altering the attachment points of the cables, one can achieve coactivation in the four-bar mechanisms with non-crossed limbs as well.

The remaining paper is organized as follows: Section 2 presents the mechanism and cable arrangement. Section 3 discusses the kinematic model of the four-bar mechanism. Section 4 derives the static model of this mechanism. Section 5 considers cables attached between the unconnected pivot pairs in the four-bar mechanisms and presents the effect of antagonistic forces on their stiffnesses with supporting experiments. Section 6 considers different cable attachment points for the mechanisms with non-crossed limbs to obtain coactivation. Finally, Section 7 presents the conclusions of this study.

2 Description of the symmetric four-bar mechanism

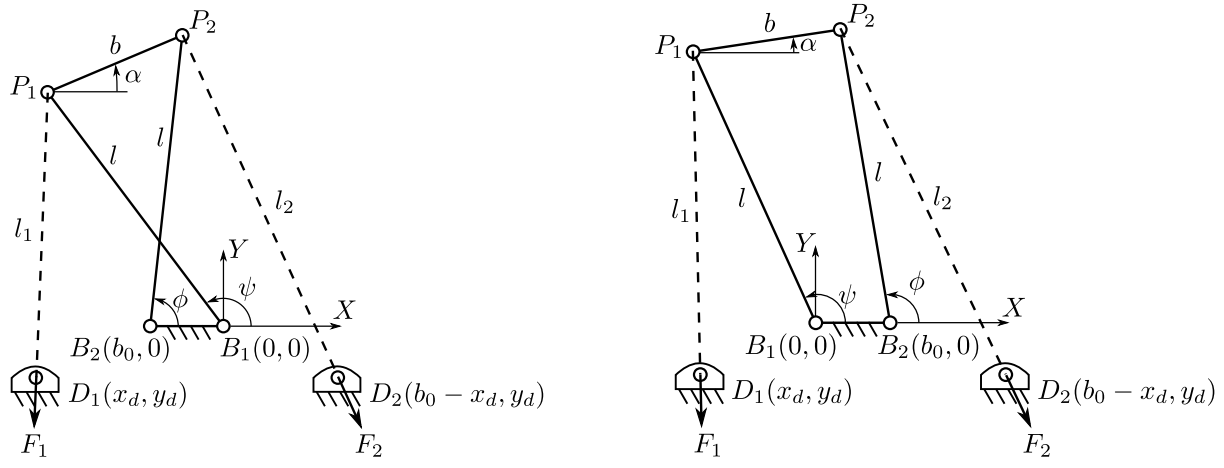

(a) $b_0 < 0$ (b) $b_0 > 0$

Fig. 1: Schematic diagram of four-bar mechanisms with symmetric limbs that are crossed when $b_0 < 0$ (left) and non-crossed when $b_0 > 0$ (right). The two actuating cables are shown in dashed lines.

The schematics of four-bar mechanisms with symmetric limbs of length l and a top bar of length b are shown in Fig. 1. The two pivots fixed to the ground are set at locations $B_1(0,0)$ and $B_2(b_0,0)$, where b_0 is a parameter that can be varied to produce different four-bar mechanisms. Notably, $b_0 < 0$ produces mechanisms with crossed limbs, while $b_0 > 0$ produces mechanisms with non-crossed limbs as illustrated in Figs. 1a and 1b, respectively. The special cases of anti-parallelogram and parallelogram mechanisms are obtained when $b_0 = -b$ and $b_0 = b$, respectively. However, the case $b_0 = 0$ degenerates the four-bar mechanism to a revolute joint and will not be considered in this work. For all the mechanisms, it is necessary that the geometric condition $\left(l > \frac{|b-b_0|}{2}\right)$ be satisfied for its assembly. Note that in the limiting assembly condition all pivots of the mechanism align and it has no finite range of movement.

This mechanism is actuated antagonistically with two cables C_1 and C_2, connected between the pivots (P_1, D_1) and (P_2, D_2), respectively, as indicated by dashed lines in Fig. 1. The position of the cable attachment pivots on the ground are parameterized as $D_1(x_d, y_d)$ and $D_2(b_0 - x_d, y_d)$ to extend the symmetry in the architecture to its actuation scheme as well. Each cable is connected to a motor fixed at the base. In this study, the motors are used as a force source only to set the specified tensions in the cables. The tension set in cable C_i is given by $F_i \geq 0$, and its varying length in the mechanism is denoted by l_i, for $i = 1, 2$. The cables are assumed to be massless and inelastic (i.e., a pure force transmission element) in this study.

The orientation of the top bar w.r.t. the base is denoted by α, while those of the two limbs w.r.t. the base are given by ϕ, ψ, respectively (see Fig. 1). The coordinate α is used to measure the range of movement of the mechanism. The upper bound for α, denoted by $\alpha_{\max}$, can be found by rotating the top bar from $\alpha = 0$ in the counterclockwise direction until the instantaneous center of rotation (i.e., the virtual intersection point of the limbs) meets with the line of an actuating cable (i.e., P_1D_1 or P_2D_2). Physically, in this configuration, the wrench imposed by one of the cables vanishes, and the static balance of the mechanism cannot be maintained. Thus, the wrench-feasible range of movement for this mechanism is given by $\alpha \in (-\alpha_{\max}, \alpha_{\max})$, owing to the symmetry in architecture and actuation scheme about $\alpha = 0$.

However, the angle α is not a valid representation of a configuration of the parallelogram mechanism $(b_0 = b)$ since it always remains zero. This mechanism will be treated separately in Section 5.1. But, for all other mechanisms, further study will be conducted inside $\alpha \in (-\alpha_{\max}, \alpha_{\max})$.

3 Kinematic model of the mechanism

The loop-closure equation for the four-bar mechanism can be written as follows (see Fig. 1):

$$\overrightarrow{B_1P_1} + \overrightarrow{P_1P_2} - \overrightarrow{B_2P_2} - \overrightarrow{B_1B_2} = \overrightarrow{0} \tag{1}$$

This can be expanded into:

$$l\begin{pmatrix}\cos\psi\\ \sin\psi\end{pmatrix} + b\begin{pmatrix}\cos\alpha\\ \sin\alpha\end{pmatrix} - l\begin{pmatrix}\cos\phi\\ \sin\phi\end{pmatrix} - \begin{pmatrix}b_0\\ 0\end{pmatrix} = \begin{pmatrix}0\\ 0\end{pmatrix} \tag{2}$$

Since the above equations are homogeneous in terms of the length parameter, they can be normalized by setting $b = 1$, without any loss of generality. Considering α as the known input, it is possible to find the trigonometric ratios of the remaining angles (ϕ, ψ) as a function of α using the above equations (see, e.g., [17], pp. 411-412). There are two possible solutions $(\phi, \psi)_1$ and $(\phi, \psi)_2$, as presented below:

$$(\phi,\psi)_1 := \begin{cases}\cos\phi = \frac{\mu\sin\alpha+\cos\alpha-b_0}{2l}\\ \sin\phi = \frac{\sin\alpha+\mu(b_0-\cos\alpha)}{2l}\\ \cos\psi = \frac{\mu\sin\alpha-\cos\alpha+b_0}{2l}\\ \sin\psi = \frac{\mu(b_0-\cos\alpha)-\sin\alpha}{2l}\end{cases} \quad (\phi,\psi)_2 := \begin{cases}\cos\phi = -\frac{\mu\sin\alpha-\cos\alpha+b_0}{2l}\\ \sin\phi = -\frac{\mu(b_0-\cos\alpha)-\sin\alpha}{2l}\\ \cos\psi = -\frac{\mu\sin\alpha+\cos\alpha-b_0}{2l}\\ \sin\psi = -\frac{\sin\alpha+\mu(b_0-\cos\alpha)}{2l}\end{cases} \tag{3}$$

where $\mu = \sqrt{\frac{4l^2-b_0^2-1+2b_0\cos\alpha}{b_0^2+1-2b_0\cos\alpha}}$. For a given $\alpha \in (-\alpha_{\max}, \alpha_{\max})$, only the configuration respecting the following two conditions must be considered. Firstly, the cables remain on the two sides of the instantaneous center of rotation. Secondly, there should be connectivity with the reference configuration $\alpha = 0$ (i.e., when P_1P_2 is parallel to B_1B_2 and remains above it).

From Fig. 1, the cable lengths (in all cases) can be written as follows:

$$\begin{cases}\text{Length of cable } C_1 \implies l_1 := \|P_1D_1\| = \sqrt{l^2 - 2lx_d\cos\psi - 2ly_d\sin\psi + x_d^2 + y_d^2}\\ \text{Length of cable } C_2 \implies l_2 := \|P_2D_2\| = \sqrt{l^2 + 2lx_d\cos\phi - 2ly_d\sin\phi + x_d^2 + y_d^2}\end{cases} \tag{4}$$

The lengths l_1, l_2 can be obtained as functions of α by substituting for the trigonometric ratios of ψ and ϕ from Eq. (3), appropriately.

4 Static model of the mechanism

The static model of the mechanism is formulated in Section 4.1 and its physical interpretation is provided in Section 4.2.

4.1 Formulation

The static model of the four-bar mechanism in Fig. 1 can be developed starting from its potential energy:

$$U = U_{\mathrm{g}} + F_1 l_1 + F_2 l_2 \tag{5}$$

where U_{g} represents the contribution of gravity and springs (if any), $F_i l_i$ with $i = 1,2$, represents the work done by the actuating cables. Treating α as the generalized coordinate in this study, differentiating U w.r.t. α and setting it to zero, yields the static equilibrium equation:

$$\frac{\mathrm{d}U_{\mathrm{g}}}{\mathrm{d}\alpha} + F_1 \frac{\mathrm{d}l_1}{\mathrm{d}\alpha} + F_2 \frac{\mathrm{d}l_2}{\mathrm{d}\alpha} = 0 \tag{6}$$

Further differentiation w.r.t. α yields the stiffness (K) of the mechanism:

$$K := \frac{\mathrm{d}^2 U_{\mathrm{g}}}{\mathrm{d}\alpha^2} + F_1 \frac{\mathrm{d}^2 l_1}{\mathrm{d}\alpha^2} + F_2 \frac{\mathrm{d}^2 l_2}{\mathrm{d}\alpha^2} \tag{7}$$

Since there are two actuation forces in a single-degree-of-freedom mechanism, there is an actuation redundancy of order 1. This redundancy allows an ∞^1 combinations of equilibrating forces (F_1, F_2) to maintain equilibrium at a given configuration α. While the mechanism moves within its limits $\alpha \in (-\alpha_{\max}, \alpha_{\max})$, it is apparent that one of the cables increases in length while the other decreases. Thus, their first-order derivatives w.r.t. α, namely $\frac{\mathrm{d}l_1}{\mathrm{d}\alpha}$ and $\frac{\mathrm{d}l_2}{\mathrm{d}\alpha}$ have opposite signs inside these limits. Since these derivatives form the coefficients of the two actuation forces in the equilibrium equation, it is apparent that the two forces are antagonistic to one another. Hence, both forces can be increased or decreased simultaneously while the mechanism is at a given α. While this change in forces preserves the configuration of the mechanism, it modifies the mechanism stiffness (K) at that configuration.

In order to understand the evolution of stiffness with the change in actuation forces at a given configuration, one can solve for F_2 from Eq. (6) and substitute into Eq. (7) to obtain:

$$K = \gamma_1 F_1 + K_g \tag{8}$$

where $\gamma_1 F_1$ represents the contribution by actuation forces and K_g (devoid of actuation forces) denotes the contribution by gravity and springs (if any). The expression of γ_1 is given by:

$$\gamma_1 = \left(\frac{\mathrm{d}^2 l_1}{\mathrm{d}\alpha^2} + \left(\frac{-\mathrm{d}l_1/\mathrm{d}\alpha}{\mathrm{d}l_2/\mathrm{d}\alpha} \right) \frac{\mathrm{d}^2 l_2}{\mathrm{d}\alpha^2} \right) \tag{9}$$

Similarly, it is also possible to solve for F_1 from Eq. (6) and substitute in Eq. (7) to obtain the coefficient of F_2 in K as:

$$\gamma_2 = \left(\frac{\mathrm{d}^2 l_2}{\mathrm{d}\alpha^2} + \left(\frac{-\mathrm{d}l_2/\mathrm{d}\alpha}{\mathrm{d}l_1/\mathrm{d}\alpha} \right) \frac{\mathrm{d}^2 l_1}{\mathrm{d}\alpha^2} \right) \tag{10}$$

Due to symmetry in the mechanism architecture and cable connections, γ_1 and γ_2 are mutually symmetric about $\alpha = 0$, i.e., $\gamma_2 = \gamma_1(-\alpha)$.

The effect of actuation forces on stiffness can be studied based on the force coefficients γ_1 and γ_2. If $\gamma_1 > 0$ (resp. $\gamma_2 > 0$), it implies that F_1 (resp. F_2) has a positive influence on the stiffness, and the antagonistic forces exhibit coactivation in

the mechanism. Similarly, if they are negative, then the forces have a negative influence on the stiffness, and there is no coactivation.

Mechanisms with positive γ_1, γ_2, are quite interesting because even when they become unstable due to external factors such as an addition of payload while the mechanism is placed vertically upward against gravity, they can be stabilized by simply increasing the actuation forces. This key property makes them ideal candidates for mimicking muscle-actuated joints in biological systems, e.g., the elbow joint of a human arm, where its increased stability can be felt by simultaneous contraction of the associated muscles.

Interestingly, the force coefficients (γ_1, γ_2) depend only on the first- and second-order derivatives of the cable lengths w.r.t. a generalized coordinate. This property shows that the coactivation ability of the mechanism is independent of other factors, such as gravity, springs, etc., although they influence the equilibrium configuration and the value of stiffness.

4.2 Physical interpretation

This sections presents more details on the static model and stiffness modulation of the mechanism by resorting to vectors and matrices. The equilibrium equation in Eq. (6) can be rewritten as follows:

$$\underbrace{\frac{\mathrm{d}U_g}{\mathrm{d}\alpha}}_{G(\alpha)} = \underbrace{\begin{bmatrix} -\frac{\mathrm{d}l_1}{\mathrm{d}\alpha} & -\frac{\mathrm{d}l_2}{\mathrm{d}\alpha} \end{bmatrix}}_{\Gamma(\alpha)} \begin{bmatrix} F_1 \\ F_2 \end{bmatrix} \tag{11}$$

From the above equation:

- **Direct static problem**: For a given set of actuation forces, Eq. (11) is a non-linear equation in α, which can admit a finite number of solutions. However, only the solution(s) that respect the limits of movement $\alpha \in (-\alpha_{\max}, \alpha_{\max})$ must be considered to ensure that the actuating cables remain on the two sides of the instantaneous center of rotation, and provide connectivity to the reference configuration $\alpha = 0$.
- **Inverse static problem**: For a given feasible configuration $\alpha \in (-\alpha_{\max}, \alpha_{\max})$, Eq. (11) becomes a linear underdetermined equation with two variables F_1, F_2. Hence, there is an ∞^1 possible combination of actuation forces that maintain the equilibrium of the mechanism.

In this study, we are only concerned with the inverse static problem.

Consider the mechanism at an equilibrium configuration $\alpha = \alpha_E$ under a given set of actuation forces (F_{1E}, F_{2E}). Suppose an external disturbance $[\Delta F_x, \Delta F_y]^\top$ is imposed at an arbitrary point $P(x,y)$ attached to the top bar, the response of the system can be characterized by linearizing the equilibrium equation around the configuration $\alpha = \alpha_E$ as follows:

$$\underbrace{\left(\frac{\mathrm{d}G}{\mathrm{d}\alpha} - \frac{\mathrm{d}\Gamma}{\mathrm{d}\alpha}\begin{bmatrix} F_1 \\ F_2 \end{bmatrix}\right)_E}_{K(\alpha_E, F_{1E}, F_{2E})} \Delta\alpha = \begin{bmatrix} \frac{\mathrm{d}x}{\mathrm{d}\alpha} & \frac{\mathrm{d}y}{\mathrm{d}\alpha} \end{bmatrix} \begin{bmatrix} \Delta F_x \\ \Delta F_y \end{bmatrix} \tag{12}$$

The coefficient of $\Delta\alpha$ is same as the expression of stiffness derived in Eq. (7). The response of the system, i.e. $\Delta\alpha$, depends on this stiffness (K). Since an ∞^1 combinations of actuation forces $[F_1, F_2]^\top$ can be applied at a given α_E, the stiffness of the system can be modulated by varying these forces. The nature of this modulation is characterized by the force coefficients γ_1, γ_2 derived in Eq. (8) in the previous section.

In the subsequent sections, the force coefficients γ_1, γ_2 are studied for various four-bar mechanisms.

5 Cable attachments at the pivots of the mechanism

As a first choice, the cable attachment pivots at the base are fixed at B_2 and B_1 for the cables C_1 and C_2, respectively. This choice is motivated by simplicity and compactness of the mechanism. Mathematically, it corresponds to setting $x_d = b_0$ and $y_d = 0$, which simplifies the cable lengths in Eq. (4) to:

$$\begin{cases} l_1 := \|P_1B_2\| = \sqrt{l^2 + b_0^2 - 2lb_0\cos\psi} \\ l_2 := \|P_2B_1\| = \sqrt{l^2 + b_0^2 + 2lb_0\cos\phi} \end{cases} \tag{13}$$

The force coefficients associated with the proposed cable arrangement is studied for the parallelogram and anti-parallelogram mechanisms in Section 5.1, and the general symmetric four-bar mechanisms in Section 5.2.

5.1 Parallelogram and anti-parallelogram mechanisms

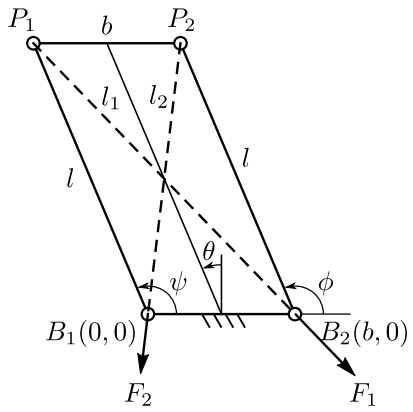

Fig. 2: Schematic of the parallelogram mechanism ($b_0 = b$).

The parallelogram mechanism, shown in Fig. 2, is obtained by setting $b_0 = b$. Unlike other four-bar mechanisms, α remains zero at all configurations for this mechanism. Hence, the orientation (θ) of the line joining mid-points of the top and base bars w.r.t. the vertical is used as the independent coordinate. The range of movement for this mechanism is limited by $\theta \in \left(-\frac{\pi}{2}, \frac{\pi}{2}\right)$, due to the flat-singularities.

From Fig. 2, it is apparent that $\phi = \psi = \frac{\pi}{2} + \theta$. Thus, from Eq. (13), the cable lengths are given by:

$$\begin{cases} l_1 = \sqrt{l^2 + b^2 + 2lb\sin\theta} \\ l_2 = \sqrt{l^2 + b^2 - 2lb\sin\theta} \end{cases} \tag{14}$$

Following the procedure in Section 4, with θ in place of α, one obtains γ_1, γ_2 as:

$$\begin{cases} \gamma_1 = -\frac{2b\lambda^2\left(\lambda^2+1\right)\cos^2(\theta)}{\left(\lambda^2+1-2\lambda\sin\theta\right)\left(\lambda^2+1+2\lambda\sin\theta\right)^{3/2}} \\ \gamma_2 = -\frac{2b\lambda^2\left(\lambda^2+1\right)\cos^2(\theta)}{\left(\lambda^2+1-2\lambda\sin\theta\right)^{3/2}\left(\lambda^2+1+2\lambda\sin\theta\right)} \end{cases} \tag{15}$$

where $\lambda = (l/b)$. Except for the leading negative signs, all the factors in the numerators of γ_1 and γ_2 are positive. The two factors in the respective denominators are also positive since they are bounded inside $[(\lambda-1)^2, (\lambda+1)^2]$ for all real θ. Thus, it is clear that $\gamma_1, \gamma_2 < 0$, which shows that antagonistic forces have a negative impact on the stiffness of the parallelogram mechanism. This result is also consistent with the experimental data presented in [18], where the cable tensions were reduced to increase the stiffness of this mechanism.

Contrary to the parallelogram mechanism, it has been proven analytically in [14] that the antagonistic forces have a positive impact on the stiffness of the anti-parallelogram mechanism.

As a numerical illustration consider parallelogram ($b_0 = b$) and anti-parallelogram ($b_0 = -b$) mechanisms with $b = 1$ m and $l = 2$ m each. For the sake of simplicity, the bar masses are neglected, and no springs are added to these mechanisms. In order to perform a fair comparison, the anti-parallelogram mechanism will also be described by the coordinate θ, as defined above for the parallelogram mechanism. The associated expressions for cable lengths and mechanism stiffness can be found in [14].

One of the ways to study the change in stiffness with increasing antagonistic forces is to specify a minimum value for the actuation forces, say $F_{\min}$. At a given configuration θ, one could compute the balancing forces (F_1, F_2) from Eq. (6) (neglecting U_g) such that one of them is equal to $F_{\min}$ while the other is greater than or equal to $F_{\min}$. These forces can be substituted in Eq. (7) to find the respective value of stiffness. This process has been carried out for different values of $F_{\min}$: 0 N, 75 N, and 150 N. The corresponding values of stiffness are plotted for the parallelogram and anti-parallelogram mechanisms in Figs. 3a and 3b, respectively. The equilibrium forces are also represented in certain configurations. It is apparent that an increase in $F_{\min}$ causes a decrease (resp. increase) in stiffness for the parallelogram (resp. anti-parallelogram) mechanism for all values of θ. This is a consequence of the negative (resp. positive) force coefficients γ_1, γ_2 for the parallelogram (resp.

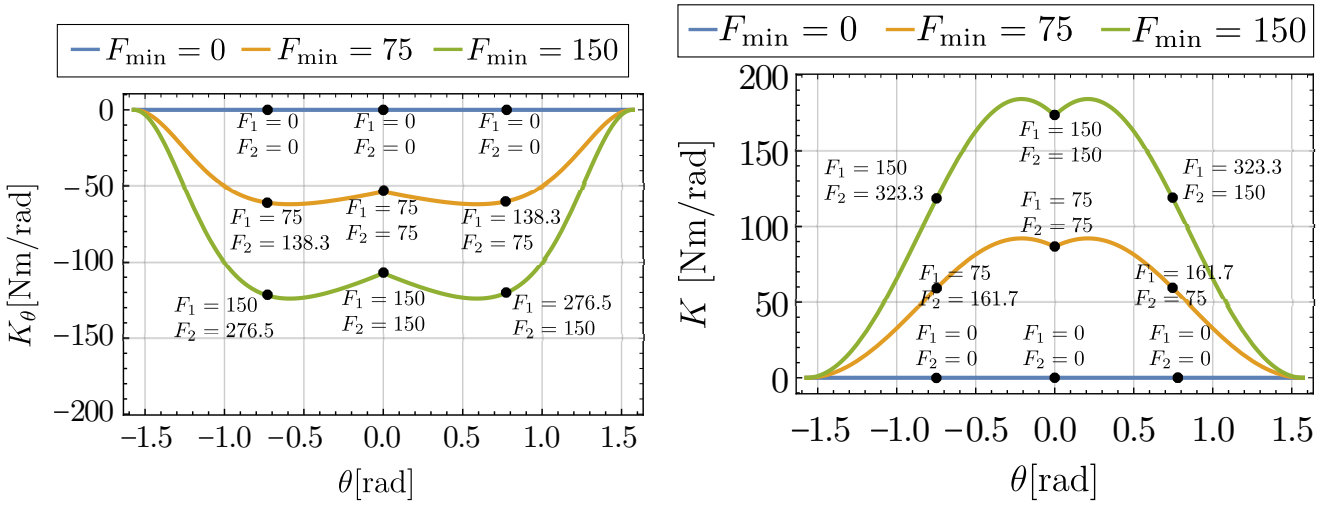

(a) Parallelogram (forces in N)

(b) Anti-parallelogram (forces in N)

Fig. 3: Stiffness of the mechanisms when $\theta \in \left(-\frac{\pi}{2}, \frac{\pi}{2}\right)$ for different actuation forces.

anti-parallelogram) mechanism. This shows that the anti-parallelogram mechanism can serve as a bio-inspired joint while the parallelogram mechanism cannot.

The coactivation properties of more general symmetric four-bar mechanisms are studied in the following section.

5.2 General symmetric four-bar mechanisms

Unlike the parallelogram and anti-parallelogram mechanisms, it is very difficult to conduct analytical studies on γ_1, γ_2 for the general mechanisms ($b_0 \neq \pm b$) due to the emergence of nested square roots in expressions of l_1, l_2 (see Eqs. (3),(13)). Hence, the nature of γ_1, γ_2 will be studied through numerical examples for these mechanisms.

Table 1: Effect of antagonistic forces on the stiffness of general symmetric four-bar mechanisms.

Condition/ Schematic	**Bounds on** $\alpha \in (-\alpha_{\max}, \alpha_{\max})$	**Plot of** γ_1 (—), γ_2 (—) **for one design with** $b = 1$ **m,** $l = 2$ **m**	$(\gamma_{\min}/b)$ **or** $(\gamma_{\max}/b)$ **in design space** $2l > (b - b_0)$ & $l \in [0, 20b]$ & $b_0 \in [0, b]$
$-b < b_0 < 0$ 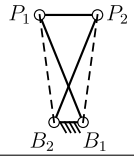	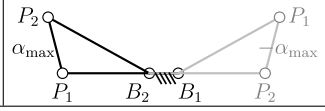	$b_0 = -0.5$ m, $\alpha_{\max} = 1.82$ rad 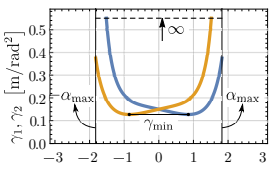	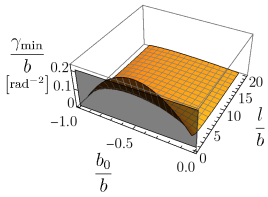
$0 < b_0 < b$ 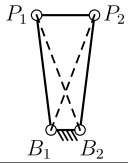	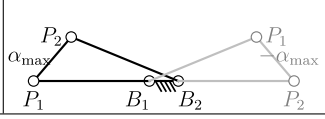	$b_0 = 0.5$ m, $\alpha_{\max} = 0.86$ rad 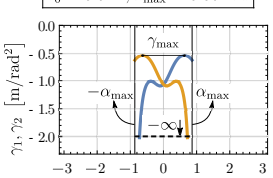	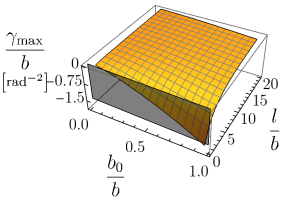

In the first version of this work [16], we considered four distinct categories of four-bar mechanisms apart from the parallelogram and anti-parallelogram architectures, depending on whether the base bar is longer/shorter than the top bar and the two limbs are crossed/non-crossed. However, the distinction based on the relative length of the base bar to the top bar is not necessary for the chosen cable attachments, as the relative kinematics and coactivation properties of a closed chain (i.e.,

the evolution of α and the cable lengths) remain invariant to the fixing of the longer or shorter bar. Indeed, this is because one mechanism is a kinematic inversion of the other (see, e.g., [19], pp. 12-14). Hence, further study in this section is conducted by setting the base bar to be smaller than the top bar, i.e., $b_0 \in [-b, b]$, with $b > 0$. The two variants of general four-bar mechanisms that emerge depending on $b_0 < 0$ and $b_0 > 0$ are considered in the following. The coactivation properties are studied numerically in these cases, and experimental validations are provided for the same in the next section.

Table 1 presents the two variants of general four-bar mechanisms. In each case, the limiting configurations at $(\pm\alpha_{\max})$, plot of γ_1, γ_2 inside $\alpha \in (-\alpha_{\max}, \alpha_{\max})$ for one candidate design, and the limiting value of γ_1, γ_2 inside the feasible design space, are presented in the successive columns of these tables. The following observations are made from them:

- The maximum orientation $(\alpha_{\max})$ of the top bar varies in $(0, \pi)$ when $b_0 < 0$, while it is limited to $(0, \frac{\pi}{2})$ when $b_0 > 0$. Thus, mechanisms with crossed limbs must be preferred for applications requiring large α.
- From the plots of γ_1, γ_2 for one candidate design, it is observed that they remain positive (resp. negative) when $b_0 < 0$ (resp. $b_0 > 0$). The values of γ_1, γ_2 tend to $\pm\infty$ near the limits due to the vanishing of $\frac{dl_1}{d\alpha}$ or $\frac{dl_2}{d\alpha}$, present in the denominator of the respective expressions (see Eqs. (9),(10)). However, this does not imply that the mechanism allows for infinite tuning of stiffness for a finite variation of actuation forces at the joint limits. It is rather indicative of the degeneracy of the wrench applied by one of the cables in that configuration. In the equilibrium equation (Eq. 6) the corresponding actuation force is no longer present due to the vanishing of its coefficient. Physically, the mechanism is not redundantly actuated at that configuration and will readily collapse when subjected to a disturbance that the remaining cable cannot balance.
- In order to verify if γ_1, γ_2 remain positive (resp. negative) for other designs when $b_0 < 0$ (resp. $b_0 > 0$), their minimum $\gamma_{\min}$ (resp. maximum $\gamma_{\max}$) inside the range of movement is tested. Since the expressions of γ_1, γ_2 are homogeneous w.r.t. the derivatives of cable lengths, one of the length variables $(b \neq 0)$ can be factored out as in Eq. (15). This reduces the design space to just two variables $(\frac{l}{b}, \frac{b_0}{b})$. Firstly, a feasible design space satisfying the assembly condition $l > \frac{b-b_0}{2}$ and bounded by $0 < \frac{|b_0|}{b} < 1$ and $0 < \frac{l}{b} \leq 20$ is constructed. The values of $\frac{\gamma_{\min}}{b}$ and $\frac{\gamma_{\max}}{b}$ are computed for several feasible designs numerically to obtain the plots in the last column of the table. From these, it is clear that $\gamma_{\min} > 0$ when $b_0 < 0$ and $\gamma_{\max} < 0$ when $b_0 > 0$. This result illustrates that the antagonistic forces have a positive (resp. negative) influence on the stiffness of four-bar mechanisms with crossed (resp. non-crossed) limbs, while the cables are attached between the unconnected pivot pairs.
- For mechanisms with $b_0 < 0$, the value of $\gamma_{\min}$ is large for designs close to the limiting assembly condition $2l = (b - b_0)$ (highlighted by gray plane in the last column of the Table 1). Recalling that the mechanism has no finite range of movement (i.e., $\alpha_{\max} = 0$ rad) at the limiting assembly condition, we observe that there is a compromise between the range of movement and the minimum value of force coefficient $(\gamma_{\min})$ for designs in the category $b_0 < 0$.

Among the four-bar mechanisms that offer coactivation (i.e., $b_0 < 0$), the anti-parallelogram mechanism $(b_0 = -b)$ has the largest range of movement $\alpha \in (-\pi, \pi)$ and is to be preferred in general. However, the other mechanisms with crossed bars might also be interesting for applications where a large orientation range may not be essential, e.g., joints in the hyper redundant robots inspired by the elephant's trunk [6].

5.3 Experimental validation

This section presents experiments on various four-bar mechanisms to confirm their ability/inability to produce coactivation. In this regard, four different mechanisms (anti-parallelogram, parallelogram, general crossed limbs, general non-crossed limbs) are considered as shown in Fig. 4. All the mechanisms have the same lengths for their base bars $|b_0| = 0.05$ m and limbs $l = 0.1$ m, while the top bar lengths are fixed at $b = 0.05$ m for the mechanisms in Figs. 4a, 4b, and at $b = 0.1$ m for the mechanisms in Figs. 4c, 4d. Two actuating cables are attached between the unconnected pairs of pivots in all the mechanisms, as highlighted by the dashed lines. They are equipped with springs on the two sides to ensure stability in the absence of actuation forces. For the mechanisms with crossed limbs shown in Figs. 4a and 4c, a pair of identical springs with stiffness 100 N/m is attached on each side parallel to the actuating cables, thereby resulting in a total stiffness of 200 N/m on either side. On the other hand, for the mechanisms presented in Figs. 4b and 4d, just one spring of stiffness 100 N/m is attached on each side with external supports. The springs are not attached parallel to the cables like in the other mechanisms due to constraints on their maximum elongation lengths.

The variation of stiffness due to actuation forces is studied at the zero orientation shown in Fig. 4, by applying equal forces on the two cables $F_1 = F_2 = F_{\text{ant}}$. Three experiments are conducted on each mechanism by setting different values of $F_{\text{ant}} = 10, 20, 30$ N. In each case, the stiffness of the mechanism is studied by applying an external force with a dynamo-meter and measuring the corresponding angular displacement with an encoder mounted on one of the moving pivots, as shown in Fig. 5. In order to enable a comparison between the results of the three experiments, the external force is regulated manually to produce the same displacement in a mechanism as observed in Fig. 5. This regulation is performed by monitoring the encoder reading in real time while applying the force. However, the value of this displacement is chosen arbitrarily in each mechanism ($\Delta\alpha \approx 25^\circ$ for anti-parallelogram, $\Delta\theta \approx 20^\circ$ for parallelgoram, $\Delta\alpha \approx 30^\circ$ for general mechanism with

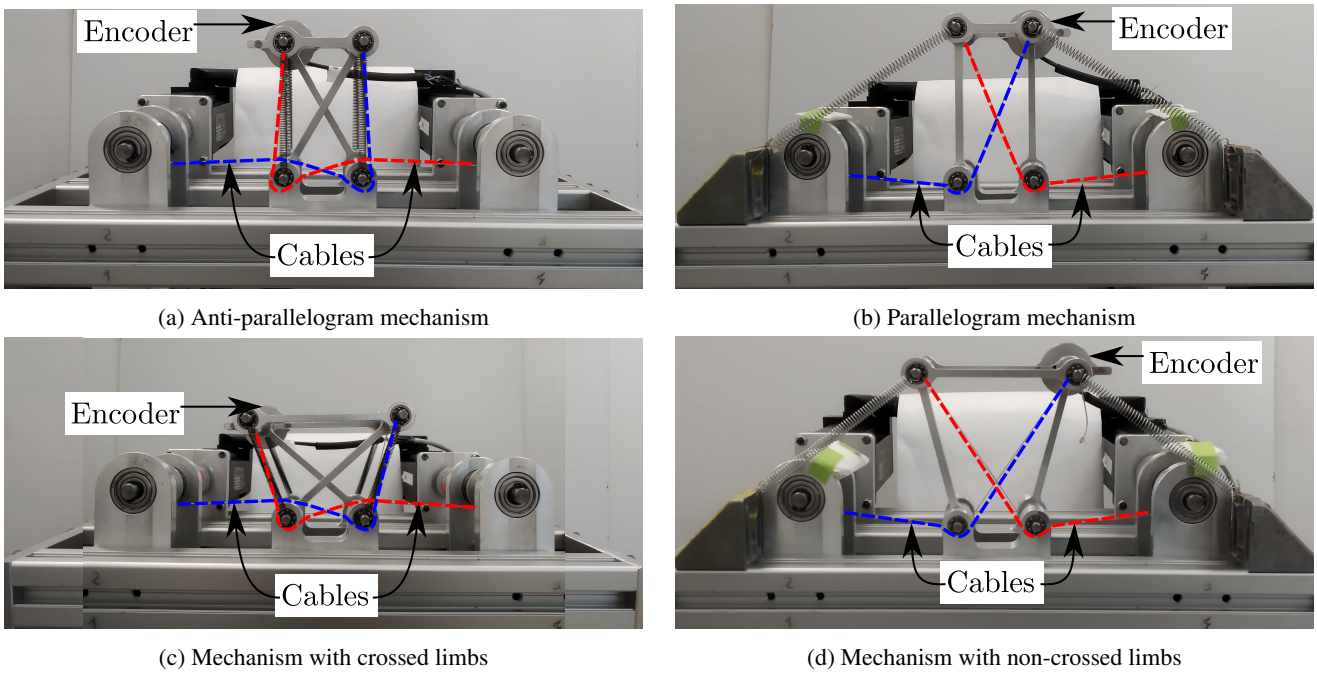

(a) Anti-parallelogram mechanism

(b) Parallelogram mechanism

(c) Mechanism with crossed limbs

(d) Mechanism with non-crossed limbs

Fig. 4: Experimental setup of different symmetric four-bar mechanisms.

crossed limbs, $\Delta\alpha \approx 15^\circ$ for general mechanism with non-crossed limbs). Large values of displacements have been chosen to overcome the frictional effects and clearly illustrate the difference in the external forces. Though such displacements cannot allow us to measure the value of stiffness exhibited by the mechanism, it can qualitatively indicate the nature of stiffness modulation by actuation forces, i.e., whether the mechanism exhibits coactivation or not. From the readings of the dynamo-meter on the left part of the figures, it is apparent that the external force required increases (resp. decreases) with the actuation force F_{ant} for mechanisms with crossed bars (resp. non-crossed bars). These results confirm that the antagonistic forces increase the stiffness of four-bar mechanisms when their limbs are crossed, while they decrease the stiffness when the limbs are non-crossed.

To further illustrate the loss of stiffness in the mechanisms with non-crossed limbs, another experiment is conducted by increasing the actuation forces $F_1 = F_2 = F_{\text{ant}}$ linearly with time. In this case, no external forces are imposed, but the mechanisms lose their stability and collapse once the force F_{ant} reaches a critical value (28.5 N for parallelogram and 55.5 N for general mechanism). The associated videos can be found in the following links for the parallelogram mechanism[1] and the general mechanism[2] with non-crossed limbs.

The next section investigates the possibility of coactivation in four-bar mechanisms with non-crossed limbs by changing their cable attachments.

6 Cable attachments to achieve coactivation in four-bar mechanisms with non-crossed limbs

Since it has been shown that the coactivation property depends only on the first- and second-order derivatives of the cable lengths, this section studies the possible cable attachments for a parallelogram mechanism and a general non-crossed limb mechanism to enable coactivation in them.

6.1 Coactivation in a parallelogram mechanism

The schematic of a parallelogram mechanism with general cable attachment points (x_d, y_d) at the base is shown in Fig. 6. In this study, we treat the coordinates (x_d, y_d) as design parameters that can be altered to obtain the desired coactivation behavior. Note that it is also possible to alter the cable attachment on the top bar from P_1 and P_2 to other points while preserving the symmetry of the mechanism. But, we do not consider this change in this study for the sake of simplicity.

The collinearity of the points points (D_i, B_i, P_i), for $i = 1, 2$, form the limits of movement of the mechanism. Clearly, the parallelogram mechanism cannot achieve its maximum orientation range of $\theta \in \left(-\frac{\pi}{2}, \frac{\pi}{2}\right)$ unless $y_d = 0$ and $x_d \neq 0$. In all other cases, the feasible range of movement will be less than π.

[1] https://youtu.be/iddUEDVTqJo
[2] https://youtu.be/Dx1eA_1-kSw

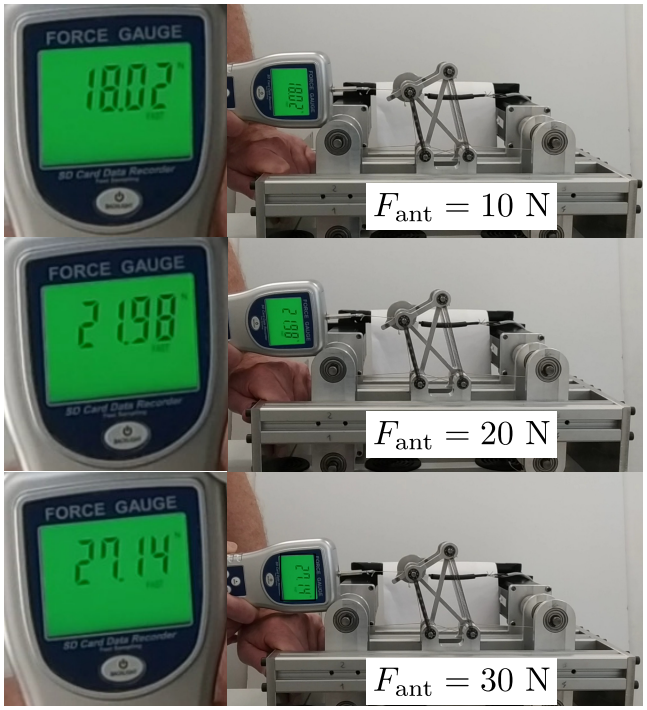

(a) Anti-parallelogram mechanism

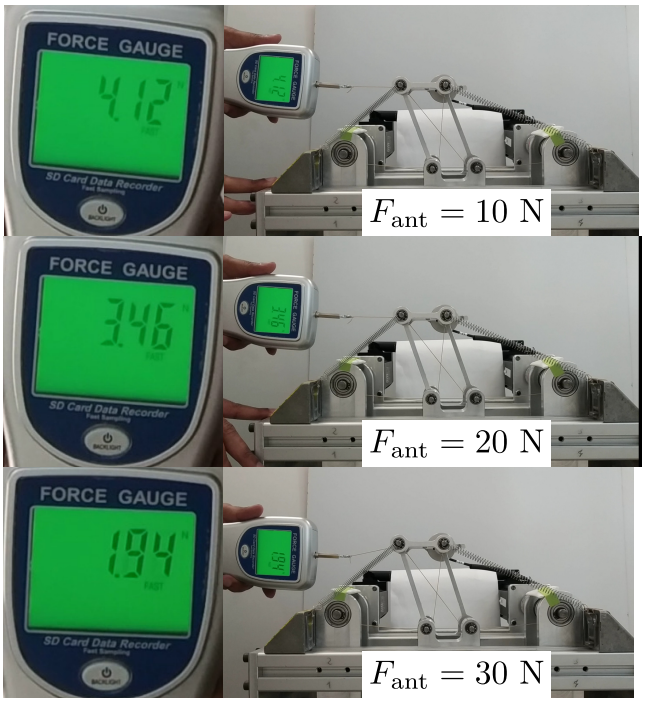

(b) Parallelogram mechanism

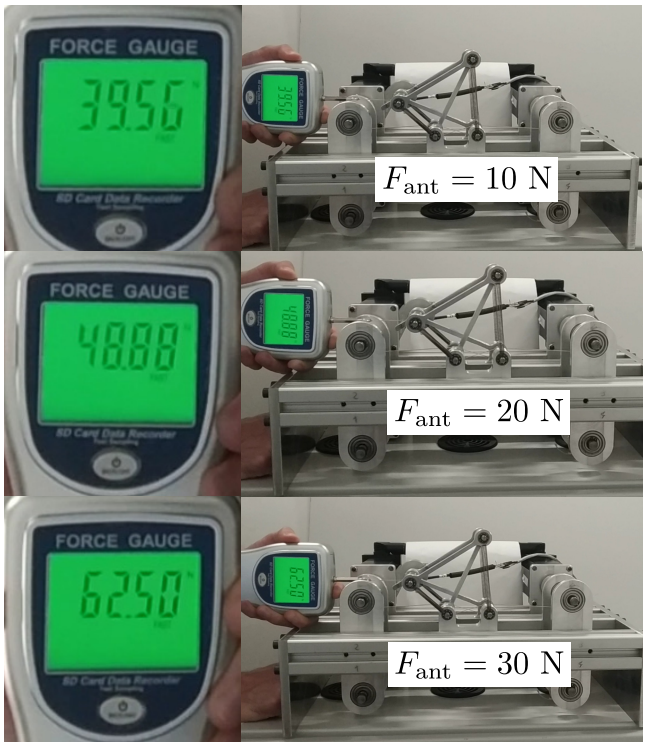

(c) Mechanism with crossed limbs

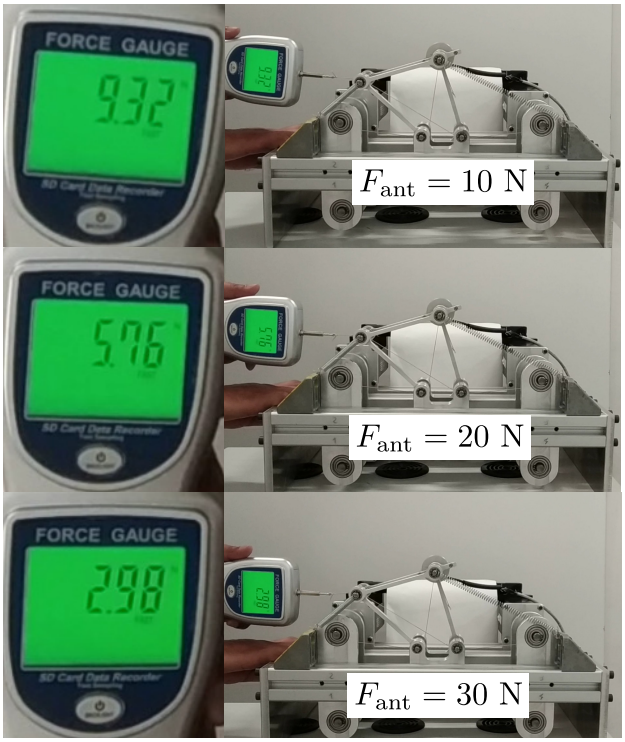

(d) Mechanism with non-crossed limbs

Fig. 5: External force required to produce the same displacement in a mechanism for different antagonistic actuation forces $F_1 = F_2 = F_{\text{ant}}$.

The cable lengths can be obtained by setting $\phi = \psi = \frac{\pi}{2} + \theta$ in Eq. (4), as follows:

$$\begin{cases} l_1 = \sqrt{l^2 + 2lx_d \sin\theta - 2ly_d \cos\theta + x_d^2 + y_d^2} \\ l_2 = \sqrt{l^2 - 2lx_d \sin\theta - 2ly_d \cos\theta + x_d^2 + y_d^2} \end{cases} \tag{16}$$

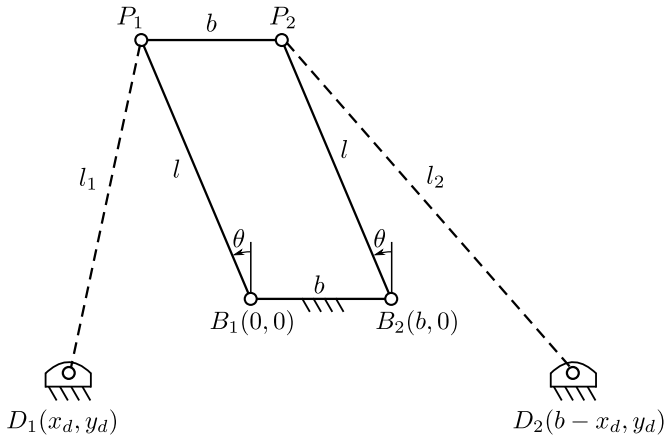

Fig. 6: Parallelogram mechanism with cables attached at points D_1 and D_2 in the base.

Note that the lengths of the cables are independent of b, indicating that the wrenches imposed by the cables, as well as the nature of coactivation, are independent of the width of the parallelogram. The force coefficients γ_1, γ_2 can be obtained from the formulae presented in Eqs. (9),(10). The expressions are not presented here due to their large sizes. But, they satisfy the symmetry condition due to configuration: $\gamma_1(x_d, y_d, -\theta) = \gamma_2(x_d, y_d, \theta)$. Additionally, due to the specific geometry of the parallelogram mechanism, they also satisfy: $\gamma_1(-x_d, y_d, \theta) = \gamma_2(x_d, y_d, \theta)$, which indicates that switching the attachment points of the cables from (D_1, D_2) to different points $\left(D_1^{'}, D_2^{'}\right)$ that are mirror images about the vertical lines placed at B_1, B_2, respectively, preserves the force coefficients in the stiffness. In addition, it can also be shown that the limits of movement remain the same while the cables are attached at (D_1, D_2) or $\left(D_1^{'}, D_2^{'}\right)$. The only difference is that the direction of the moment imposed by the respective cable changes between the two scenarios.

In order to achieve coactivation with the parallelogram mechanism, the force coefficients γ_1, γ_2 must be positive. However, since their expressions are difficult to analyze analytically, we consider γ_1 for one configuration $(\theta = 0)$ of the mechanism as follows:

$$\gamma_1(\theta = 0) = \frac{2l(y_d - l)\left(y_d(y_d - l) + x_d^2\right)}{\left((l - y_d)^2 + x_d^2\right)^{3/2}} \tag{17}$$

It is apparent that the denominator is always positive. Hence, the condition to achieve coactivation at $\theta = 0$, i.e. $\gamma_1(\theta = 0) > 0$, can be written as:

$$\gamma_1(\theta = 0) > 0 \implies \begin{cases} \text{Always}, & \text{when } (y_d > l) \\ (x_d^2 + (y_d - (l/2))^2 - (l/2)^2) < 0, & \text{when } (y_d < l) \end{cases} \tag{18}$$

Thus, the limiting boundaries of attachment point $D_1(x_d, y_d)$ are formed by a circle and a straight line to achieve coactivation in a parallelogram mechanism. As an illustration, the feasible region for the attachment point D_1 is shown along with the mechanism for the parameters $l = 1, b = 2$, in Fig. 7. Note that the scale of the mechanism has been normalized w.r.t. l without any loss of generality. As explained above, for every attachment point D_1 that is chosen on the left half of the feasible space, there is a point $D_1^{'}$ that offers the same joint limits and force coefficients for the resulting mechanism (see Fig. 7). The choice between them can be made based on secondary factors such as compactness or ease of motor placement.

For further study, we choose two points $D_{1a} = (-1, 2)$ and $D_{1b} = (-2/5, 2/5)$ inside the feasible region as shown in Fig. 7. The schematic of the resulting mechanisms with cable attachment points and the plots of γ_1, γ_2 inside their respective joint limits are presented for D_{1a} in Fig. 8 and for D_{1b} in Fig. 9. In both cases, we observe that the force coefficients remain positive inside their joint limits, indicating that both attachment points offer coactivation at all feasible configurations of the parallelogram mechanism, similar to mechanisms with crossed limbs. Since the attachment point D_{1b} is closer to the limiting boundary than D_{1a} (see Fig. 7), the associated values of force coefficients are smaller near $\theta = 0$ (see Figs. 8b and 9b). However, as a compromise, the attachment at D_{1b} offers a larger range of movement for the mechanism than its counterpart. Hence, the designer must choose the attachment points appropriately depending on which feature is more significant for the task.

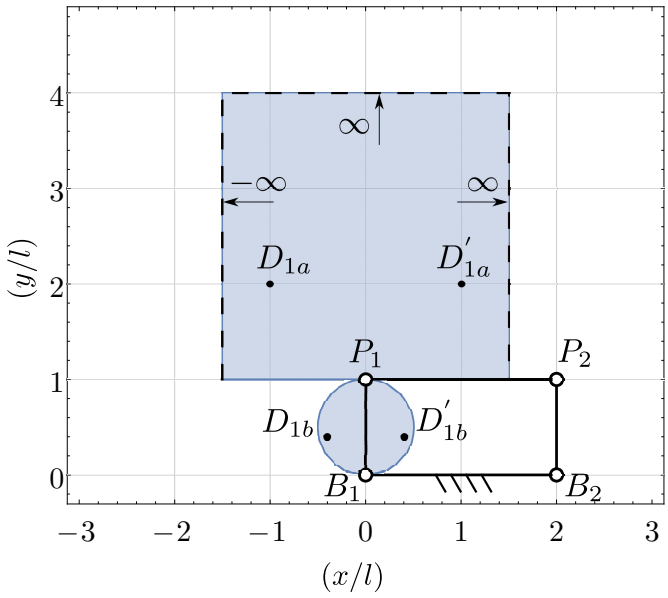

Fig. 7: Feasible region for the cable attachment point D_1 to achieve coactivation at the configuration $\theta = 0$ rad in the parallelogram mechanism with $l = 1, b = 2$.

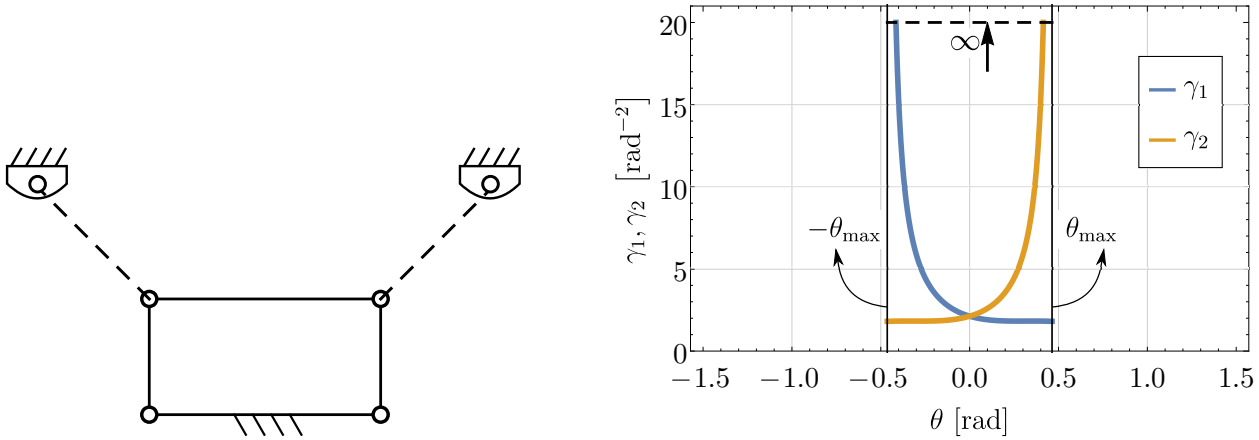

(a) Mechanism with cable attachment points

(b) Variation of force coefficients inside the joint limits

Fig. 8: Parallelogram mechanism with $l = 1, b = 2$ and its force coefficients when the left (resp. right) cable is attached to $D_{1a} = (-1, 2)$ (resp. $D_{2a} = (3, 2)$) at the base. The limits of movement are found to be $\pm\theta_{\max} = \pm 0.46$ rad. The force coefficient γ_1 (resp. γ_2) tends to infinity asymptotically as θ approaches the limit $-\theta_{\max}$ (resp. $\theta_{\max}$).

6.2 Coactivation in a general four-bar mechanism with non-crossed limbs

This section considers a four-bar mechanism with non-crossed limbs with geometry $l = 1, b = 1, b_0 = 1/2$. As in the previous section, the cable attachment points at the base are parameterized by (x_d, y_d) coordinates while retaining the attachment points at P_1 and P_2 in the top bar. From Eq. (4), the lengths of the cables are recalled below:

$$\begin{cases} l_1 = \sqrt{l^2 - 2lx_d \cos\psi - 2ly_d \sin\psi + x_d^2 + y_d^2} \\ l_2 = \sqrt{l^2 + 2lx_d \cos\phi - 2ly_d \sin\phi + x_d^2 + y_d^2} \end{cases} \tag{19}$$

Unlike in the parallelogram mechanism, the presence of intermediate angles (ψ, ϕ) (see Fig. 1) ensures that all the bar lengths are involved in the expressions of cable lengths. Further, the force coefficients γ_1, γ_2 are computed using the formulae in Eqs. (9),(10). The symmetry due to configuration α, i.e., $\gamma_1(x_d, y_d, \alpha) = \gamma_2(x_d, y_d, -\alpha)$ is respected, but there is no symmetry w.r.t. the sign of coordinate x_d as observed in the previous section.

For this mechanism, the condition for coactivation (i.e., positivity of force coefficients) at one configuration $\alpha = 0$ is

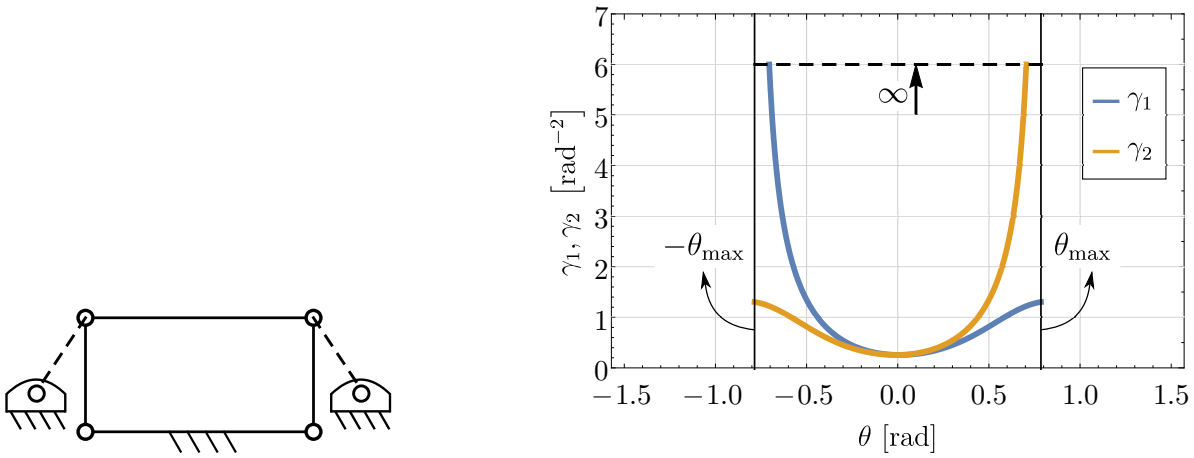

(a) Mechanism with cable attachment points

(b) Variation of force coefficients inside the joint limits

Fig. 9: Parallelogram mechanism with $l = 1, b = 2$ and its force coefficients when the left (resp. right) cable is attached to $D_{1b} = (-2/5, 2/5)$ (resp. $D_{2b} = (12/5, 2/5)$) at the base. The limits of movement are found to be $\pm\theta_{\max} = \pm 0.79$ rad. The force coefficient γ_1 (resp. γ_2) tends to infinity asymptotically as θ approaches the limit $-\theta_{\max}$ (resp. $\theta_{\max}$).

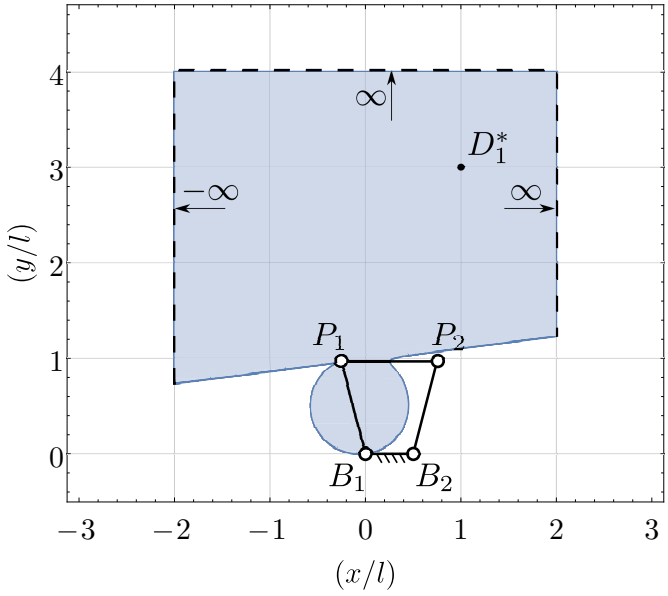

Fig. 10: Feasible region for the cable attachment point D_1 to achieve coactivation at the configuration $\alpha = 0$ rad in a four-bar mechanism with non-crossed limbs of geometry $l = 1, b = 1, b_0 = 1/2$.

itself quite large to be analyzed symbolically. Hence, its geometry parameters $l = 1, b = 1, b_0 = 1/2$ are substituted to derive a simplified condition in terms of x_d and y_d as follows:

$$-\sqrt{15}x_d^3 + x_d^2\left(31y_d - 8\sqrt{15}\right) - x_d\left(\sqrt{15}y_d^2 - 8y_d + \sqrt{15}\right) + y_d\left(31(y_d^2+1) - 16\sqrt{15}y_d\right) > 0 \tag{20}$$

The above expression does not factor into simpler terms like the previous case. Hence, the region satisfying the above condition (i.e., the feasible region for attachment point D_1) has been plotted as is, along with the mechanism in Fig. 10.

One feasible candidate $D_1^* = (1, 3)$ has been chosen for this mechanism. As explained in the previous section, there exist limits of movement due to the collinearity of the points (D_i, B_i, P_i). These limits are found to be $\alpha \in (-\alpha_{\max}, \alpha_{\max})$ with $\alpha_{\max} = 0.31$ rad. The schematic of the mechanism with the chosen attachment points for the cables is shown in Fig. 11a, and the respective plot of the force coefficients within the joint limits is presented in Fig. 11b. It is observed that γ_1, γ_2 are both positive, indicating that the mechanism exhibits coactivation throughout the entire range of movement.

The above results show that it is possible to achieve coactivation in the parallelogram mechanism and general four-bar

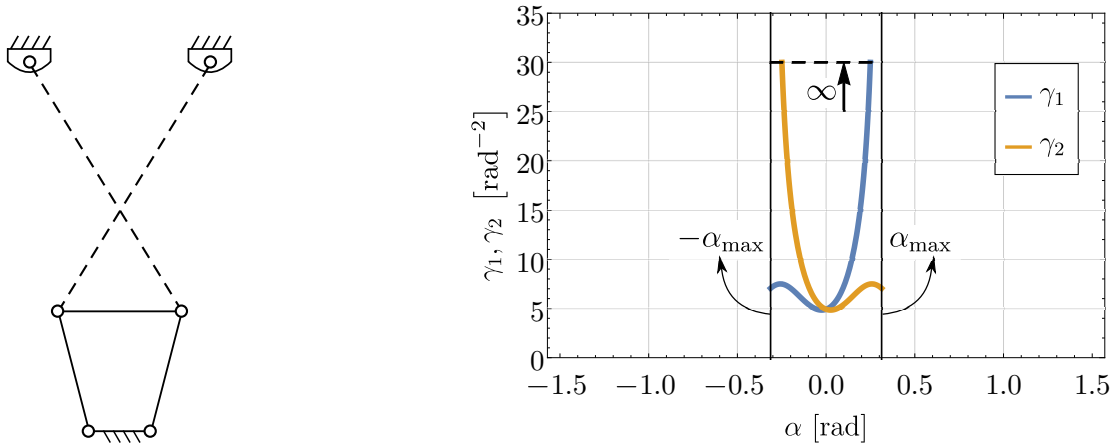

(a) Mechanism with cable attachment points

(b) Variation of force coefficients inside the joint limits

Fig. 11: Four-bar mechanism with $l = 1, b = 1, b_0 = 1/2$ and its force coefficients when the left (resp. right) cable is attached to $D_1^* = (1,3)$ (resp. $D_2^* = (-1/2,3)$) at the base. The limits of movement are found to be $\pm\alpha_{\max} = \pm 0.31$ rad. The force coefficient γ_1 (resp. γ_2) tends to infinity asymptotically as α approaches the limit $\alpha_{\max}$ (resp. $-\alpha_{\max}$).

mechanisms with non-crossed limbs by selecting appropriate cable attachment points. However, there is a compromise on the range of movement permissible for the mechanism.

7 Conclusion

A class of four-bar mechanisms with symmetric limbs, actuated antagonistically with two symmetrically attached cables imposing forces $F_1, F_2 > 0$, was considered in this work. The effect of an actuation force F_1 (resp. F_2) on the stiffness of a mechanism was studied through its coefficient γ_1 (resp. γ_2) in the expression of stiffness after eliminating the other force F_2 (resp. F_1) using the equilibrium equation. The expressions of force coefficients showed that they depend only on the varying cable lengths and its first- and second-order derivatives w.r.t. a generalized coordinate. Also, due to the symmetry in architecture and arrangement of cables, the force coefficients are mutually symmetric about the configuration where the top and base bars are parallel. When γ_1, γ_2 are positive, the stiffness increases with the increase in cable forces, similar to the muscle actuation of a biological joint, and the mechanism is said to exhibit coactivation.

As a first arrangement, the cables were attached between the two unconnected pairs of pivots in the four-bar mechanism. It was found through numerical simulations that $\gamma_1, \gamma_2 > 0$ occurs only when the two limbs are crossed, and not otherwise. Among such mechanisms, the anti-parallelogram mechanism offers the largest orientation range of $(-\pi, \pi)$ for the top bar w.r.t. its base, and is thus best suited for building bio-inspired robot manipulators. The other mechanisms with crossed limbs might also be of interest for applications where a large range of movement is not a necessity, as in redundant and hyper-redundant systems. These results were validated by experiments.

Further investigations were conducted on the possibility of coactivation in four-bar mechanisms with non-crossed limbs by changing the attachment points of the cables. Numerical examples of a parallelogram mechanism and a general mechanism with non-crossed limbs showed that there exist suitable attachment points to produce coactivation in these mechanisms, but it comes at the cost of a reduced range of movement.

In the future, this study will be extended to multiple degree-of-freedom mechanisms suitable for mimicking biological joints, such as an elbow in the human arm or intervertebral contact in a bird's neck.

8 Acknowlegments

The authors would like to thank Nicolas Testard, Stéphane Jollivet, Philippe Lemoine, and Denis Creusot for their contribution to the experimental set-up.

References

[1] G. Boucher, T. Laliberté, and C. Gosselin, "Mechanical design of a low-impedance 6-degree-of-freedom displacement sensor for intuitive physical human–robot interaction," *Journal of Mechanisms and Robotics*, vol. 13, no. 2, 2021.

[2] P. Palmieri, M. Melchiorre, and S. Mauro, "Design of a lightweight and deployable soft robotic arm," *Robotics*, vol. 11, no. 5, p. 88, 2022.

[3] F. Liu, W. Xu, H. Huang, Y. Ning, and B. Li, "Design and analysis of a high-payload manipulator based on a cable-driven serial-parallel mechanism," *Journal of Mechanisms and Robotics*, vol. 11, no. 5, 2019.
[4] A. Niikura, H. Nabae, G. Endo, M. Gunji, K. Mori, R. Niiyama, and K. Suzumori, "Giraffe neck robot: First step toward a powerful and flexible robot prototyping based on giraffe anatomy," *IEEE Robotics and Automation Letters*, vol. 7, no. 2, pp. 3539–3546, 2022.
[5] M. Furet, A. Abourachid, C. Böhmer, V. Chummun, C. Chevallereau, R. Cornette, X. De La Bernardie, and P. Wenger, "Estimating motion between avian vertebrae by contact modeling of joint surfaces," *Computer Methods in Biomechanics and Biomedical Engineering*, vol. 25, no. 2, pp. 123–131, 2022.
[6] Y. Liu, Z. Ge, S. Yang, I. D. Walker, and Z. Ju, "Elephant's trunk robot: An extremely versatile under-actuated continuum robot driven by a single motor," *Journal of Mechanisms and Robotics*, vol. 11, no. 5, 2019.
[7] V. Parenti-Castelli and N. Sancisi, "Synthesis of spatial mechanisms to model human joints," in *21st Century Kinematics* (J. M. McCarthy, ed.), (London), pp. 49–84, Springer London, 2013.
[8] A. Hamon, Y. Aoustin, and S. Caro, "Two walking gaits for a planar bipedal robot equipped with a four-bar mechanism for the knee joint," *Multibody System Dynamics*, vol. 31, pp. 283–307, 2014.
[9] S. Levin, S. L. de Solórzano, and G. Scarr, "The significance of closed kinematic chains to biological movement and dynamic stability," *Journal of Bodywork and Movement Therapies*, vol. 21, no. 3, pp. 664–672, 2017.
[10] S. Burgess, "A review of linkage mechanisms in animal joints and related bioinspired designs," *Bioinspiration & Biomimetics*, vol. 16, no. 4, p. 041001, 2021.
[11] M. L. Latash, "Muscle coactivation: definitions, mechanisms, and functions," *Journal of Neurophysiology*, vol. 120, no. 1, pp. 88–104, 2018.
[12] B. Vanderborght, A. Albu-Schaeffer, A. Bicchi, E. Burdet, D. Caldwell, R. Carloni, M. Catalano, O. Eiberger, W. Friedl, G. Ganesh, M. Garabini, M. Grebenstein, G. Grioli, S. Haddadin, H. Hoppner, A. Jafari, M. Laffranchi, D. Lefeber, F. Petit, S. Stramigioli, N. Tsagarakis, M. Van Damme, R. Van Ham, L. Visser, and S. Wolf, "Variable impedance actuators: A review," *Robotics and Autonomous Systems*, vol. 61, no. 12, pp. 1601–1614, 2013.
[13] Z. Li, W. Chen, J. Zhang, Q. Li, J. Wang, Z. Fang, and G. Yang, "A novel cable-driven antagonistic joint designed with variable stiffness mechanisms," *Mechanism and Machine Theory*, vol. 171, p. 104716, 2022.
[14] V. Muralidharan and P. Wenger, "Optimal design and comparative study of two antagonistically actuated tensegrity joints," *Mechanism and Machine Theory*, vol. 159, p. 104249, 2021.
[15] V. Muralidharan, N. Testard, C. Chevallereau, A. Abourachid, and P. Wenger, "Variable stiffness and antagonist actuation for cable-driven manipulators inspired by the bird neck," *Journal of Mechanisms and Robotics*, vol. 15, no. 3, 2023.
[16] V. Muralidharan, C. Chevallereau, P. Wenger, and N. J. S. Testard, "Effect of antagonistic cable actuation on the stiffness of symmetric four-bar mechanisms," in *Cable-Driven Parallel Robots* (S. Caro, A. Pott, and T. Bruckmann, eds.), (Cham), pp. 332–343, Springer Nature Switzerland, 2023.
[17] J. M. McCarthy and G. S. Soh, *Geometric Design of Linkages*. New York: Springer-Verlag, 2 ed., 2010.
[18] Q. Boehler, S. Abdelaziz, M. Vedrines, P. Poignet, and P. Renaud, "Towards the control of tensegrity mechanisms for variable stiffness applications: A case study," in *New Trends in Mechanism and Machine Science* (P. Wenger and P. Flores, eds.), (Cham), pp. 163–171, Springer International Publishing, 2017.
[19] A. Ghosh and A. K. Mallik, *Theory of Mechanisms and Machines*. New Delhi: Affiliated East-West Press Private Limited, 3 ed., 1998.